Cancer Immunology, Immunotherapy (2021) 70:2179–2195
https://doi.org/10.1007/s00262-020-02792-5

ORIGINAL ARTICLE

Tumor-draining lymph nodes are survival niches that support T cell priming against lymphatic transported tumor antigen and effects of immune checkpoint blockade in TNBC

Meghan J. O'Melia[1] · Margaret P. Manspeaker[2,3] · Susan N. Thomas[1,2,4,5]

Received: 15 July 2020 / Accepted: 7 November 2020 / Published online: 18 January 2021

Abstract

Triple negative breast cancer (TNBC) is a significant clinical problem to which immunotherapeutic strategies have been applied with limited success. Using the syngeneic E0771 TNBC mouse model, this work explores the potential for antitumor $CD8^+$ T cell immunity to be primed extratumorally in lymphoid tissues and therapeutically leveraged. $CD8^+$ T cell viability and responses within the tumor microenvironment (TME) were found to be severely impaired, effects coincident with local immunosuppression that is recapitulated in lymphoid tissues in late stage disease. Prior to onset of a locally suppressed immune microenvironment, however, $CD8^+$ T cell priming within lymph nodes (LN) that depended on tumor lymphatic drainage remained intact. These results demonstrate tumor-draining LNs (TdLN) to be lymphoid tissue niches that support the survival and antigenic priming of $CD8^+$ T lymphocytes against lymph-draining antigen. The therapeutic effects of and $CD8^+$ T cells response to immune checkpoint blockade were furthermore improved when directed to LNs within the tumor-draining lymphatic basin. Therefore, TdLNs represent a unique potential tumor immunity reservoir in TNBC for which strategies may be developed to improve the effects of ICB immunotherapy.

Keywords Triple-negative breast cancer · Lymph nodes · Tumor dissemination · Immune checkpoint blockade · T cell priming · Drug delivery

Introduction

Breast cancer is the most common cancer among women worldwide [1, 2] making it a significant public health threat. Triple negative breast cancer (TNBC) is the most aggressive breast cancer type with the poorest outcomes due to its high propensity to metastasize and limited available treatment modalities [3]. As such, there is a clear need for improved therapies to treat TNBC. Immunotherapy has emerged as one of the most promising strategies to combat TNBC due to its potential to treat focal as well as disseminated disease and the fact that TNBC is a relatively immunogenic breast cancer type. Immune checkpoint blockade (ICB) is an immunotherapy class that can re-energize anergic and exhausted T cells by inhibiting signaling that dampens the cytotoxic functions of T lymphocytes [4]. Atezolizumab, a mAb against programmed cell death (PD) ligand 1 (PDL1) [5] is the only currently approved ICB strategy for a subset of TNBC patients [6]. However, rates of response are

Electronic supplementary material The online version of this article (https://doi.org/10.1007/s00262-020-02792-5) contains supplementary material, which is available to authorized users.

✉ Susan N. Thomas
susan.thomas@gatech.edu

1 Wallace H. Coulter Department of Biomedical Engineering, Georgia Institute of Technology and Emory University, IBB 2310, 315 Ferst Drive NW, Atlanta, GA 30332, USA

2 Parker H. Petit Institute for Bioengineering and Bioscience, Georgia Institute of Technology, Atlanta, GA 30332, USA

3 School of Chemical and Biomolecular Engineering, Georgia Institute of Technology, Atlanta, GA 30332, USA

4 George W. Woodruff School of Mechanical Engineering, Georgia Institute of Technology, Atlanta, GA 30332, USA

5 Winship Cancer Institute, Emory University, Atlanta, GA 30332, USA

severely limited overall (~ 16%) [6]. Improving immunotherapy therefore represents a critical hurdle to diminishing TNBC mortality.

Although its effects are elicited within the tumor microenvironment (TME), antitumor immunity in TNBC can appear extratumorally [7–9]. This suggests the potential for approaches leveraging such extratumoral microenvironments to improve ICB. To this end, secondary lymphoid tissues, including spleens and lymph nodes (LNs), are organs that house a substantial fraction of the cells of the adaptive immune system and are specialized to facilitate antigen presentation and lymphocyte priming, activation, and expansion [10, 11]. Lymphoid tissues of TNBC patients have been shown to house tumor-specific lymphocytes [7], although whether these cells locally expand in response to antigen or infiltrate after antigenic priming elsewhere remains ill-defined. Although spleens access antigen in the circulation, sampling of antigen within LNs is facilitated by the transport functions of the lymphatic system. Lymph, which contains solute and small, nanoscale particulate (10–50 nm)-laden interstitial fluid, is formed in the periphery and is drained through lymphatic vessels into downstream LNs where it is accessed by resident antigen presenting cells [12–17]. Antigen presenting cells within peripheral tissues also facilitate antigen access by phagocytosing antigen and migrating to these draining LN (dLN) where they can interact with lymphocytes [18–21]. Whether splenic access to tumor-derived factors in the circulation and lymphatic transport from mammary tissue to LNs are influenced by malignancy to regulate the lymphoid tissue immune microenvironment, however, is poorly understood. Moreover, lymphoid tissues, like the TNBC TME, have been reported to be immunosuppressed: regulatory T cells (Tregs) and myeloid-derived suppressor cells (MDSC) are increased in the TME and pre-metastatic TdLN environments of TNBC patients [22–26]; dendritic cells (DCs) and effector T cells also tend to be dysfunctional in the human TNBC TME [27, 28]. However, increased quantity and quality of $CD8^+$ T cell infiltration into the tumor increases survival [29–31], and enhanced $CD8^+$ T cell-DC interactions with the TdLN are associated with enhanced survival in TNBC patients [32]. Likewise, TdLN-resident macrophages have been shown to enhance antitumor responses in TNBC [9]. The potential for lymphoid tissues to not only access tumor antigen but facilitate priming of tumor-specific immunity that has functional antitumor effects thus remains poorly defined.

Herein, the potential for lymphoid tissues to support extratumoral lymphocyte priming was evaluated in the syngeneic mouse model of E0771 TNBC. The results suggest that despite TNBC disease that manifests in TME-localized immune suppression and disrupts tumor vascular functions that regulate antigen access to antigen presenting cells, LNs within the tumor lymphatic drainage basin, e.g., TdLNs, are lymphoid tissue niches that support the survival and antigenic priming of $CD8^+$ T lymphocytes. TdLNs therefore represent a unique potential tumor immunity reservoir that when therapeutically targeted can improve the effects of ICB immunotherapy.

Materials and methods

Cell culture E0771 and E0771-OVA (kind gift of Dr. Zachary Harman, Duke University) mouse mammary carcinoma cells were cultured in Dulbecco's Modified Eagle Medium with 10% heat-inactivated fetal bovine serum and 1% penicillin/streptomycin/amphotericin B from Life Technologies (Carlsbad, CA, USA), the latter with the addition of 1 µg/mL puromycin (Gibco Laboratories, Gaithersburg, MD, USA).

Animal tumor models C57/Bl6 (either CD45.2 or CD45.2) mice were purchased at 6 week of age from the Jackson laboratory (Bar Harbor, Maine, USA). All protocols were approved by the Institutional Animal Care and Use Committee. The hair on the skin over the fourth (inguinal) mammary fatpad was removed using depilatory cream (Church & Dwight, Ewing Township, NJ, USA) and cleaned using warm water and ethanol wipes. For tumor-bearing cohorts, 0.5×10^6 E0771 or E0771-OVA cells were injected into the fourth (inguinal) mammary fatpad of 6–8 week old mice on day 0. Tumor dimensions were measured with calipers in three dimensions and reported as an ellipsoidal volume.

Flow cytometry analysis Excised LNs were incubated in 1 mg/mL Collagenase D (Sigma-Aldrich) in D-PBS with calcium and magnesium for 75 min at 37 °C, passed through a 70 µm cell strainer (Greiner Bio-One, Monroe, NC, USA), washed, and resuspended in a 96 well plate (VWR International, Inc.) for staining. Spleen capsules were disrupted using 18G needles and the cells suspension was passed through a 70-µm cell strainer, pelleted by centrifuging at 350G for 5 min then incubated with red blood cell lysis buffer (Sigma-Aldrich) for 7 min at room temperature, diluted with D-PBS, washed, and resuspended in 1 mL D-PBS. 50 µL of the resulting solution was plated for staining. Tumors and mammary fatpad tissues were mechanically disrupted using 18 G needles, then incubated in 1 mg/mL collagenase D (Sigma-Aldrich) in D-PBS with calcium and magnesium for 4 h at 37 °C, passed through a 70 µm cell strainer (Greiner Bio-One), washed with D-PBS, pelleted, and plated. All antibodies for flow cytometry were from Biolegen, Inc. (San Diego, CA, USA). Cells were blocked with antimouse CD16/CD32 (2.4G2) (Tonbo Biosciences, San Diego, CA, USA) for 5 min on ice, then washed. Cells were stained with fixable viability dye Zombie Aqua (1:100, Biolegend, Inc.) for 30 min at room temperature, then washed with D-PBS with calcium and magnesium. Antibodies were prepared in flow cytometry buffer (D-PBS with calcium and

magnesium + 1% bovine serum albumin (Sigma-Aldrich) at the following dilutions based on preliminary titrations: PerCP-Cy5.5 antimouse CD45.2 (1.25:100) or BV711 antimouse CD45.2 (1.25:100), PerCP antimouse CD3 (2.5:100) or BV711 antimouse CD3 (1.25:100), APC-Cy7 antimouse CD8 (2.5:100), AF700 antimouse CD25 (1:100), BV786 antimouse PD-1 (1.25:100), PE-Cy7 antimouse CD39 (5:100), BV605 antimouse Tim3 (1.25:100), and BV421 antimouse CD44 (5:100). Cells were incubated with antibody solution for 30 min on ice in the dark, then washed with flow cytometry buffer. Cells were fixed and permeabilized using Foxp3/Transcription Factor Staining Buffer Set (Thermo Fisher Scientific, Inc.) per manufacturer instructions. Tcf1 staining solution was made using PE antimouse Tcf1 (Beckton Dickinson) at a concentration of 1.25:100 in permeabilization buffer. Cells were resuspended in Tcf1 staining solution and incubated for 75 min on ice in dark, then washed with flow cytometry buffer. Cells were resuspended in flow cytometry buffer and kept at 4 °C until analyzed with a customized BD LSRFortessa (BD Biosciences). Compensation was performed using UltraComp and ArC compensation beads (Thermo Fisher Scientific, Inc.), and the data analyzed using FlowJo software v10 (FlowJo, LLC, Ashland, OR, USA).

$CD8^+$ T cell isolation OT-I animals were purchased from Charles River Laboratories (Lyon, France) and bred in-house. OT-I animals were sacrificed and the spleens harvested and disrupted using 18G needles followed by washing with D-PBS. Cells were passed through a cell strainer (Greiner Bio-One, Monroe, NC, USA), washed with D-PBS, and incubated with ACK Lysing Buffer (Lonza Group AG, Basel, Switzerland) for 60 s at room temperature, quenched with D-PBS, washed with D-PBS, and resuspended for counting. Cells were resuspended at 10^8 cells/mL buffer (2% bovine serum albumin in D-PBS), blocked with Normal Rat Serum, and mixed with $CD8^+$ T cell isolation antibody cocktail (Stem Cell Technologies, Vancouver, Canada), followed by streptavidin-coated magnetic beads (Stem Cell Technologies, Vancouver, Canada). Buffer was added to the mixture, and placed in a magnet (Stem Cell Technologies, Vancouver, Canada), and the supernatant collected. Cells were then counted and resuspended in carboxyfluorescein succinimidyl ester (CFSE; Life Technologies), and then quenched with RPMI 1640 medium (Life Technologies) containing 10% heat-inactivated fetal bovine serum (Life Technologies). Purity, viability, and CFSE loading were confirmed via flow cytometry on a customized LSRFortessa flow cytometer (Becton Dickinson, Franklin Lakes, NJ, USA) before adoptive transfer.

Adoptive transfer Isolated $CD8^+$ T cells were suspended in sterile saline at a concentration of 1×10^6 cells/200 µL sterile saline. The hair over the neck of the mice was removed using depilatory cream, cleaned using warm water, and ethanol wipes, and suspended cells injected intravenously (i.v.) via the jugular vein.

Micro-computed tomographic imaging Animals were perfused with saline at the heart followed by neutral buffered formalin (Thermo Fisher Scientific, Inc.) for 10 min, then with saline to rinse, and lastly MicroFil (Flow Tech Inc., Carver, MA) catalyzed at a viscosity appropriate for small vessels (5 mL lead-based contrast agent: 2.5 mL diluent: 0.25 mL curing agent). Afterwards, perfused mice were carefully stored at 4 °C overnight to cure the contrast agent. The following day, mammary fatpad or tumor samples were harvested and stored in D-PBS. Microcomputed tomographic imaging was accomplished using a SCANCO Medical µCT50 (SCANCO USA, Inc., Wayne, PA, USA). µCT image slices were constrained using manual selection of the sample outline and processed with a Gaussian filter at a consistent global threshold via the SCANCO Medical µCT Evaluation Program before 3-dimensional reconstruction [33].

Enzyme-linked immunosorbence assay The R&D Systems DuoSet ELISA kit (Minneapolis, MN, USA) was used for ELISA assays. In brief, Nunc MaxiSorp high affinity plates (Thermo Fisher, Inc.) were incubated with capture antibody overnight at room temperature. The plate was washed with 0.05% tween (Sigma-Aldrich) in D-PBS (wash buffer), and then blocked with 1% bovine serum albumin in D-PBS (reagent diluent). Plates were washed, and 100uL sample diluted in reagent diluent were added to each well and incubated for 2 h at room temperature, then washed. The detection antibody was added to each well and incubated for 2 h at room temperature, then washed. Streptavidin–HRP was added to each well and allowed to incubate for 20 min at room temperature, followed by addition of substrate solution (R&D Systems, Minneapolis, MN, USA). 2 N sulfuric acid (VWR Chemicals BDH, Radnor, PA, USA) was used to stop the reaction, and the absorbance read at 450 nm, 540 nm, and 570 nm on a BioTek Synergy H4 Hybrid Multimode Microplate Reader (Winooski, VT, USA).

Fluorescent tracers 500 nm red fluorescent (580/605 excitation/emission) carboxylate-modified microspheres were purchased from Thermo Fisher Scientific, Inc. 10,000 Da (Dalton) Alexa Fluor 647 dextran was purchased from Thermo Fisher Scientific, Inc. 500,000 Da amino-dextran (Thermo Fisher Scientific, Inc.) was covalently labeled by incubation with Alexa Fluor 700-NHS-Ester dye (Thermo Fisher Scientific, Inc.) in 0.1 M $NaHCO_3$ at pH 8.4 for 4 h on a tube rocker. AF700 dextran–dye conjugates were purified from unreacted free dye by Sepharose CL-6B gravity column chromatography after conjugation. Purified dextran–fluorophore conjugates were further confirmed free of unconjugated dye by a second Sepharose CL-6B column analysis [16]. All reagents were used and maintained under sterile conditions. Hydrodynamic sizes were confirmed

pre-injection by dynamic light scattering using a Zetasizer Nano ZS (Malvern Instruments, Ltd., Malvern, U.K.).

Tracer injections Fluorescent tracers suspended in saline were co-infused by syringe pump at a rate of ~ 300 nL/s directly into the center of the tumors for tumor-bearing groups, or into the mammary fatpad for naïve groups, using a 31 gauge needle while mice were under anesthesia using isoflurane. 500 nm red fluorescent microspheres (19 pM), 30 nm AF700 (4.8 µM), and 10 nm AF647 dextran (4.8 µM) were co-infused in 20 µL of saline total. Mice were euthanized via CO_2 asphyxiation at the prescribed times post-tracer injection for each experiment.

Tracer biodistribution analyses At 4, 24, and 72-h post-tracer injection, mice were sacrificed and the tumor or mammary fatpad injection site, mammary fatpad-draining and contralateral non-draining inguinal and axillary LNs, spleen, lungs, liver, and kidneys were harvested and homogenized with a FastPrep-24 Automated Homogenizer. Whole tissue homogenate fluorescence was measured with a Synergy H4 BioTek plate reader (BioTek Instruments, Inc., Winooski, VT, USA), compensation was applied, and fluorescent tracer amounts, and concentrations were calculated from standard curves made by spiking individual tissue homogenates with tracer solution.

LN mapping Naïve or day 11 E0771-bearing C57/Bl6 mice were injected with 30 nm AF647 dextran in the center of the tumor or the fourth (inguinal) mammary fatpad. Animals were sacrificed 24 h later, and LNs imaged on a LI-COR Odyssey imaging system (Lincoln, NE, USA).

mAb biodistribution aPD1 mAb was mixed with either *N*-hydroxysuccinimide ester-AlexaFluor610, AlexaFluor647, or AlexaFluor700 (Thermo) at 6 molar excess for 6 h. Fluorophore-labeled mAbs were cleaned of free dye using 7 kDa MWCO Zeba spin columns, suspended in sterile saline, and mAb concentration determined by bicinchoninic acid assay (Thermo). Mice were intradermally (i.d.) injected in the forearm or flank or alternatively i.v. via the jugular vein with each of the three dye-labeled mAb, varying the site of each dye with each mouse, to ensure that labeling did not impact accumulation. 24 h after administration, the inguinal, axial, and brachial LNs contralateral and ipsilateral to the i.d. injection site was excited, homogenized, and fluorescence analyzed as described above.

Therapeutic evaluation E0771 tumors were implanted on day 0 and measured using calipers every 48 h beginning at day 3. On day 11 of tumor growth, 100 µg of aPD1 mAb (BioXCell) was administered in one of three injection routes: i.d. in the flank to target the inguinal (primary) TdLN, i.d. in the forearm to target the axial (secondary) TdLN, or i.v. via the jugular vein. Isotype control mAb was administered i.d. in the flank in control animals. Animals were randomized and researchers blinded until sacrifice 5 d later, when lymphocytes were analyzed as described above.

Statistical analysis The data are represented as the mean accompanied by SEM, and statistics were calculated using GraphPad Prism 6, 7, and 8 software (GraphPad Software, Inc., La Jolla, CA, USA). Statistical significance was defined as $p < 0.05$, 0.01, 0.005, and 0.001, respectively, unless otherwise specified. Area under the curve (AUC) was calculated using the built-in Prism analysis tool.

Results

E0771 mammary tumor growth is associated with TME-localized immune suppression and vascular remodeling

Quantities of various TILs within E0771 tumors implanted in the mammary fatpad were evaluated at various stages of E0771 tumor progression (Fig. 1a). Lymphocytes ($CD45^+$), particularly T cells, infiltrated the TME at early stages, but their numbers within the TME progressively decreased during tumor growth (Fig. 1b), in line with reports of initial immune responses in human patients deteriorating in late-stage disease [28]. At these later tumor stages, however, the number of PDL1 expressing $CD45^+$ and $CD45^-$ cells within the TME were strongly increased (Fig. 1c), a trend recapitulating those seen in advanced human disease [34, 35]. Total DC ($CD45^+CD11c^+B220^-CD3^-$) levels within the TME trended towards a reduction in infiltration at all analyzed stages (Fig. 1b), whereas Treg and MDSC levels increased significantly (~ tenfold higher) relative to the naïve tissue (Fig. 1c).

Priming of tumor antigen-specific $CD8^+$ T cells (Fig. S1) was evaluated in two stages of E0771 tumor growth in order to delineate the influence of disease stage on TME-localized antitumor immunity. As such, CFSE labeled OT-I cells were adoptively transferred into CD45.1 animals bearing E0771-OVA tumors at either early (d7) or late (d21) stage (Fig. S2). Tracing of proliferative response by monitoring CFSE dilution revealed tumor antigen-specific proliferation of tumor-infiltrating T cells to be attenuated in d21 as compared to d7 tumors (Fig. 1d, e), peaking at 3 generations (three divisions) for d7 tumors and 1 generation (1 division) for d21 tumors 96 h post-adoptive transfer. Cell viability of all proliferating cells was also severely diminished at both tumor stages (Fig. 1d, f). Cells that had not proliferated (G0) were more likely to remain viable (Fig. 1f), indicating that activation or proliferation processes contributed to cell death in this tissue [36–38]. Unproliferated, tumor antigen-specific $CD8^+$ T cells in d21 tumors also exhibited significantly reduced viability as compared to those infiltrating d7 tumors (Fig. 1f), further demonstrating the suppressive environment in late stage tumors. Thus, tumor-antigen-specific T cells in the TME show limited proliferation and low viability which

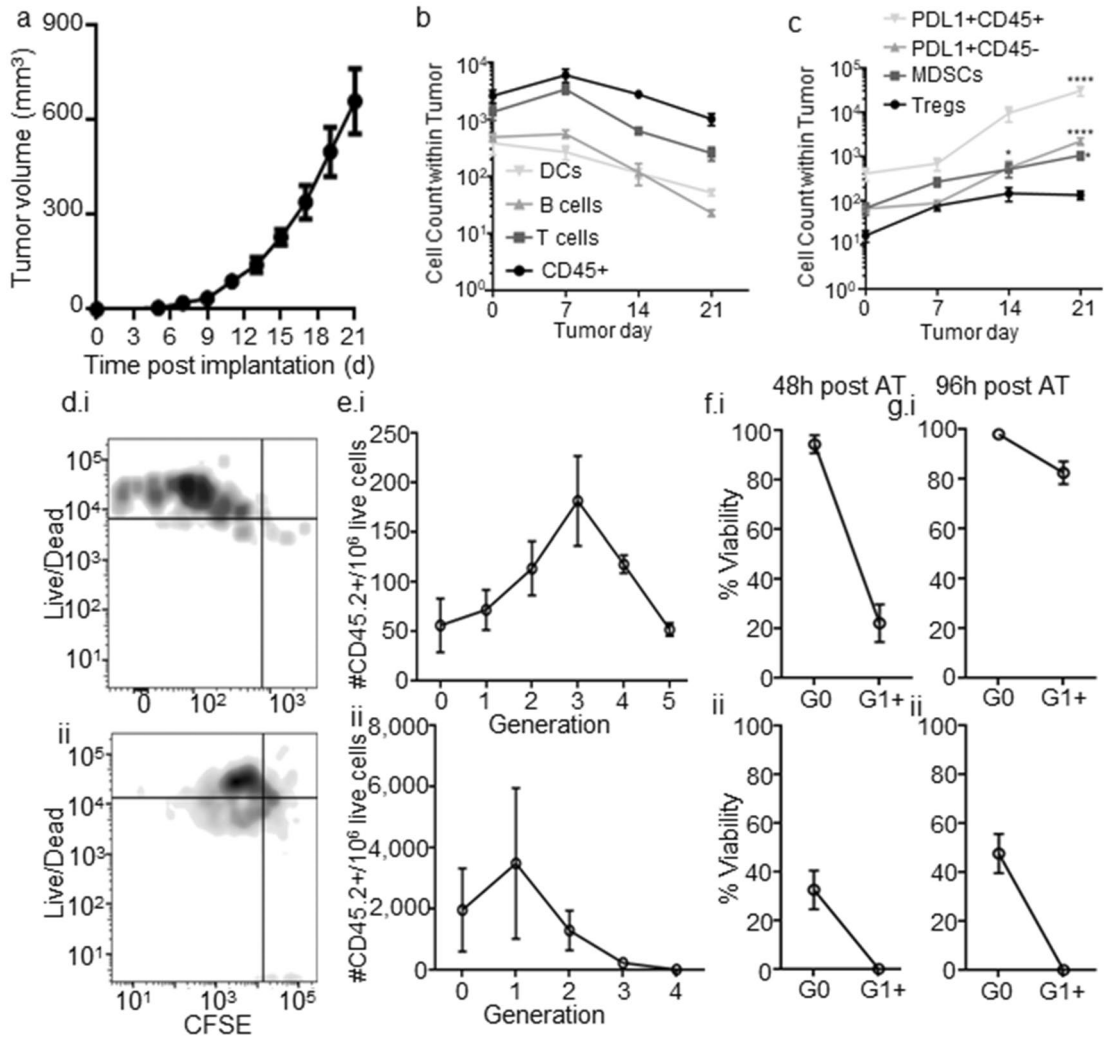

Fig. 1 The tumor immune microenvironment remodels throughout E0771 disease progression and supports poor priming and viability of tumor antigen-specific CD8+T cells. **a** E0771 tumor growth after implantation in the 4th mammary fatpad. **b**, **c** Number of major [CD45+; DC, CD45+CD11c+B220−CD3−; B cells (CD45+B220+CD11c−CD3−); T cells (CD45+CD3+B220−)] (**b**) and immunosuppressive [PDL1+CD45+; PDL1+CD45−; MDSC (CD45+CD11b+Gr1+); Tregs (CD45+CD3+B220−CD4+CD8−FoxP3+CD25+)] (**c**) immune cell subsets in TME. Representative CFSE versus live/dead staining (**d**) and quantification of number of live (**e**) and % viable (**f**–**g**) CD45.2+CD3+CD8+ donor T cells adoptively transferred OT-I cells within TME in each proliferative generation in d7 (**i**) or 21 (**ii**) CD45.1 E0771-OVA tumor-bearing mice 48 (**d**–**f**) or 96 (**g**) h post-transfer. *Significance by two-way ANOVA with Tukey comparison; #Significance against theoretical value of 1.0 by one-sample *t* test; $n = 5$–6 mice

progressively worsens with disease progression, coinciding with localized immunosuppression (Fig. 1c).

Remodeling of the tumor vasculature, another cancer hallmark [39, 40], in the E0771 model was also evaluated. uCT analyses of perfused tumors at various times post-implantation revealed the vasculature to expand throughout tumor development and progression (Fig. 2a), as indicated by measured vascular volume (Fig. 2b), surface area (Fig. 2c), and relative vascular volume compared to total tissue volume (Fig. 2d), and most substantially so in late stage (d21) disease. These changes were accompanied by an increase in tumor levels of vasoendothelial growth factor-A (VEGF-A), an angiogenic growth factor both broadly implicated in neoangiogenesis and the regulation of vascular permeability [41–44] as well as highly expressed and associated with poor survival in TNBC [45–47] (Fig. 2e). The mammary fatpad concentration of VEGF-C, a lymphangiogenic growth factor that modulates lymphatic drainage functions [48, 49] and in melanoma has been implicated in regulating immune microenvironments [50], also decreased with the presence of a tumor, but did not progressively diminish with disease progression (Fig. 2f). The tumor vasculature of TNBC E0771

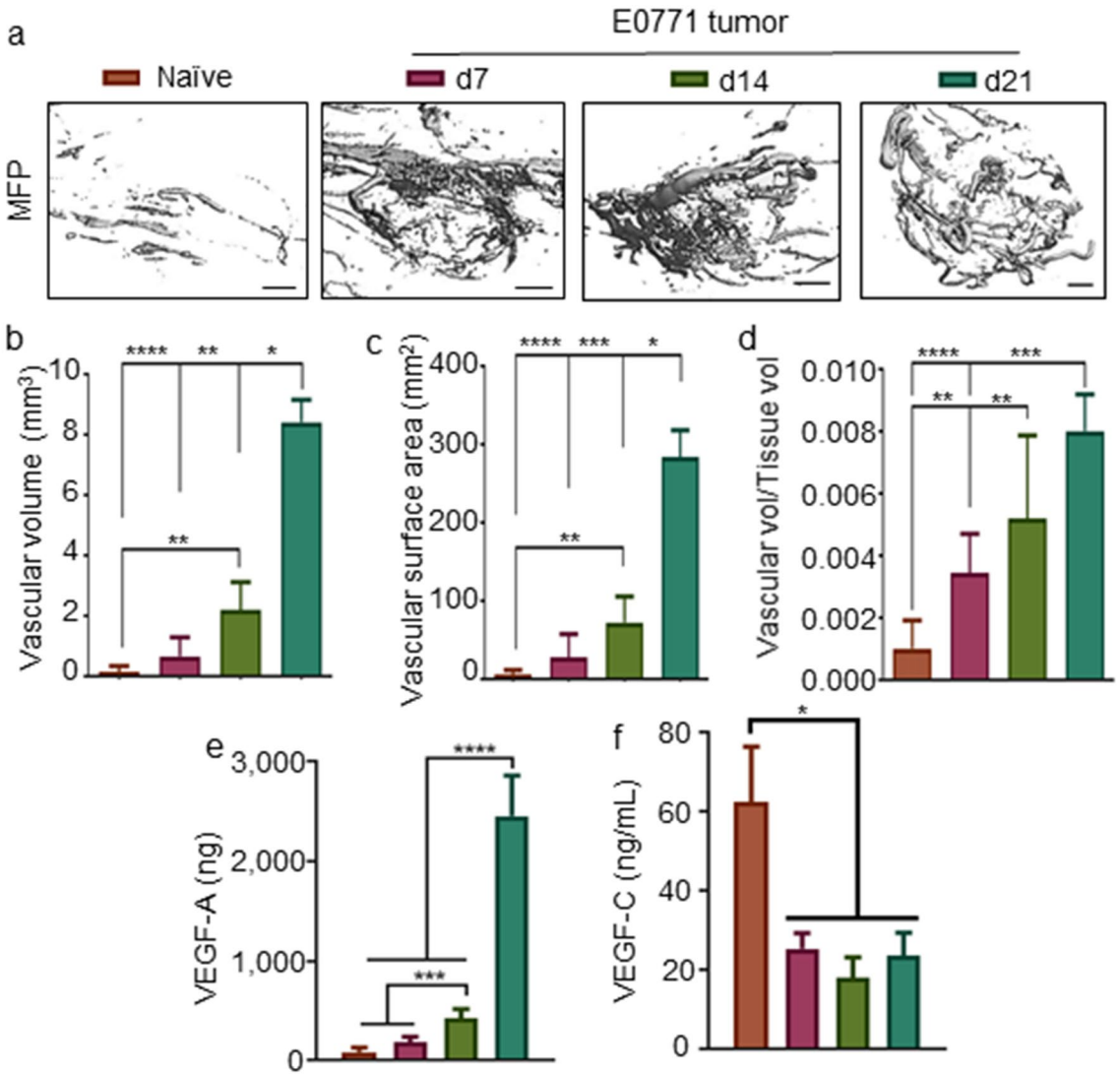

Fig. 2 The tumor vasculature remodels throughout E0771 disease progression. Representative images (**a**) and quantification of mean vascular volume (**b**), vascular surface area (**c**), and vessel diameter (**d**) of micro-computed tomography 3D reconstructions of the mammary fatpad or E0771 tumors. VEGF-A (**e**) and VEGF-C (**f**) levels in the naïve or tumor-bearing mammary fatpad throughout disease progression. *Significance by two-way ANOVA with Tukey comparison; #Significance against theoretical value of 1.0 by one-sample *t* test; $n = 5$–6 mice; scale bar indicates 1 mm

tumors thus concurrently remodels with the tumor immune microenvironment throughout disease progression.

E0771 disease progression effects on lymphoid tissue immune microenvironments and molecular dissemination from the TME

Given the potential for the complex molecular and cellular crosstalk between tumors and lymphoid tissues [7, 9, 12, 16, 32, 51–55] to be influenced by tumor vascular remodeling (Fig. 2) and reports of immune suppressive features in lymphoid tissues and in circulation of human patients [22–26], the immune microenvironments of lymphoid tissues in the E0771 model were evaluated. First, mapping of the mammary fatpad drainage was performed by tracing of fluorescent signal of injected fluorescent tracer (Fig. S3) into various LNs, which identified inguinal LNs ipsilateral to the mammary fatpad as the sentinel (primary) TdLN (Fig. S4). Major cell subtypes in this TdLN or the non-draining contralateral inguinal LN (NdLN) as well as spleen were found to remain largely unchanged throughout tumor progression (Fig. 3a–c). In the TdLN, however, levels of cells exhibiting immune suppressive phenotypes, including MDSCs, Tregs, and PDL1 expressing $CD45^+$ cells, remained relatively consistent across disease stage (Fig. 3d). However, the abundance of $PDL1^+CD45^-$ cells,

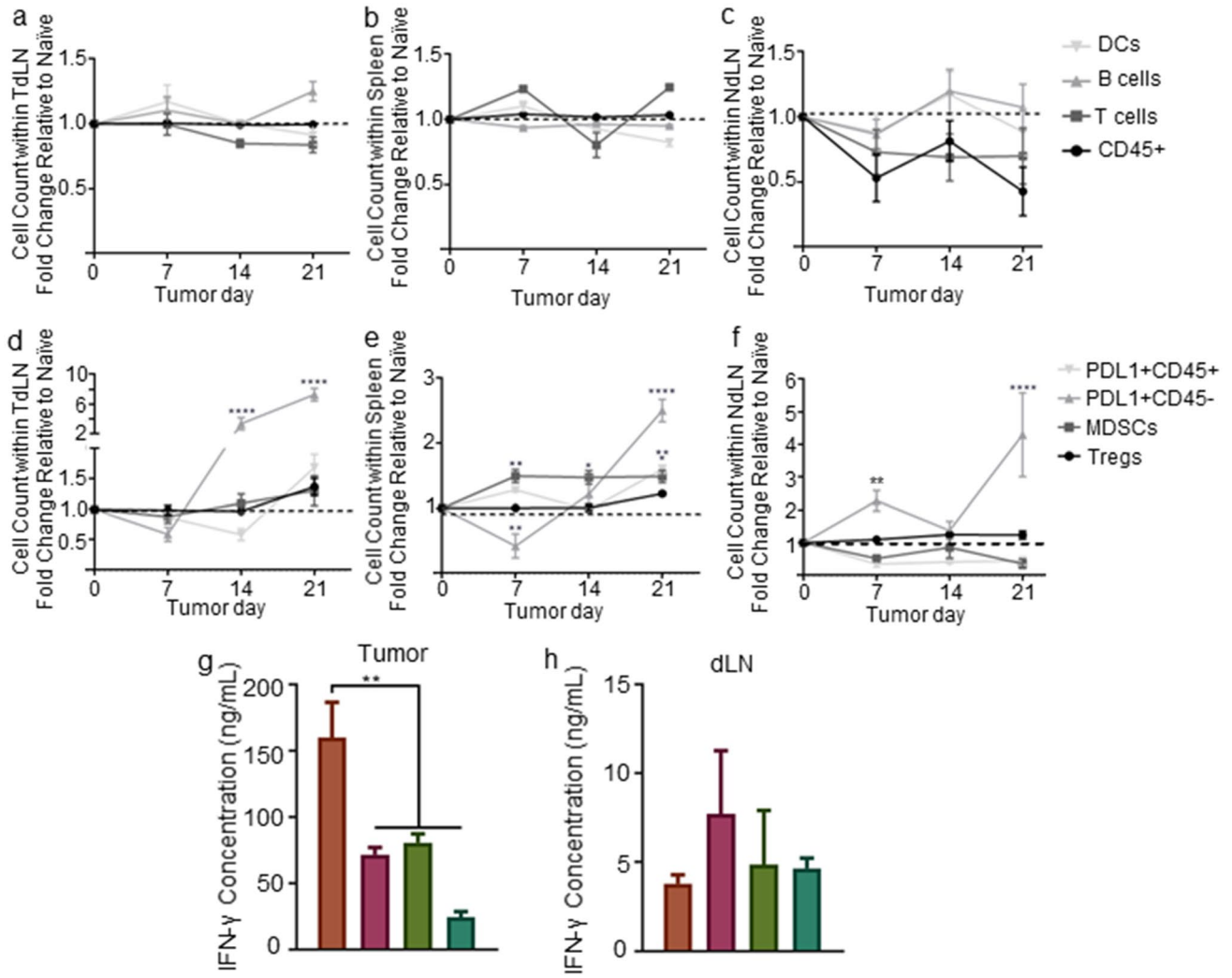

Fig. 3 Changes in lymphoid tissue immune microenvironments during E0771 progression. Fold change in the relative number of immune [CD45+; DC, CD45+CD11c+B220−CD3−; B cells (CD45+B220+CD11c−CD3−); T cells (CD45+CD3+B220−)] (**a, b**) and immunosuppressive [PDL1+CD45+; PDL1+CD45−; MDSC (CD45+CD11b+Gr1+); Tregs (CD45+CD3+B220−CD4+CD8−FoxP3+CD25+)] (**d–f**) cell subsets in the dLN (**a**, **d**), spleen (**b**, **e**), and NdLN (**c**, **f**) relative to naïve tissue; IFN-γ concentration in the tumor (**g**) and dLN (**h**) microenvironments throughout disease progression. *Significance by two-way ANOVA with Tukey comparison (**a–f**) or one-way ANOVA with Tukey comparison (**g–h**); $n = 5–6$ mice

which manifest as a result from either LN metastasis or stromal cell expression of PDL1, was increased in later stages (Fig. 3d). Overall, TdLNs were largely spared of tumor-induced immunosuppression, particularly in early stage disease. Spleens of tumor-bearing animals, in contrast, demonstrated increased MDSC levels even at early disease stage (d7), alterations that persists throughout disease progression (Fig. 3e). Levels of non-hematopoietic cells expressing PDL1 were found to decline in d7 tumor bearing animals but progressively increase in later stages (Fig. 3e). Levels of $CD45^+$ cells expressing PDL1 also increased in spleens of d21 tumor bearing animals. The spleen thus demonstrates immunosuppression, albeit at lower levels as compared to the tumor, beginning at the commencement of tumor development and progression. In the NdLN, levels of non-hematopoietic cells expressing PDL1 increase progressively, while other immunosuppressive cells, including MDSCs and Tregs, trend towards decreasing below levels seen in the naïve mammary fatpad (Fig. 3f). Of note, PDL1 expression in tumors exists in a regulatory loop controlled by $CD8^+$ T cell production of interferon-γ (IFN-γ) [56]. As such, we measured IFN-γ in both the tumor and dLN microenvironments, and found that the presence of a tumor decreased IFN-γ concentration within the mammary fatpad (Fig. 3g), while IFN-γ concentration was maintained at similar levels within the dLN throughout tumor development and progression (Fig. 3h). Thus, we interpret this PDL1 expression levels

as being tumor-intrinsic immunosuppression and not due to increased $CD8^+$ T cell presence or activation in the TME.

Remodeling of these lymphoid tissue microenvironments are suggestive of crosstalk with the E0771 TME that is disease stage dependent. To reveal if disease-associated tumor remodeling (Figs. 1, 2, 4a) impacts on dissemination from the TME into lymphoid tissues is associated with differences in immune suppression within lymphoid tissues that result from disease, we utilized a panel of differently sized tracers labeled with fluorophores with minimal spectral overlap to simultaneously probe various mechanisms of molecular dissemination from the mammary fatpad though fluorescence quantification of harvested, homogenized tissues (Figs. 4a, S3, S5). Macromolecules permeable to the blood vasculature rapidly diffuse through the tumor interstitium to be cleared into the blood whereas those larger are instead retained within the interstitium. If smaller than the approximate tissue pore size, macromolecules are subjected to interstitial flows to be drained to and taken up within lymphatic vasculature, in contrast to larger macromolecules and particulates that are instead locally retained and cleared in their intact form into lymphatic tissues only by the actions of phagocytic antigen presenting cells (Fig. S5a). A panel of tracers consisting of 5 versus 30 and 500 nm tracers (Fig. S5b) were thus used to probe blood versus lymphatic clearance pathways, respectively, and the latter pair delineating passive lymphatic drainage versus cell-mediated trafficking. This cocktail of tracers was infused into the naïve mammary fatpad as a single injection, and fluorescent content in different tissues assessed 4, 24, and 72 h later to confirm expected size- and time-dependent distribution profiles. 500, but not 5 or 30, nm tracers were found to be retained at the injection tissue at high levels (Fig. S5c). With respect to

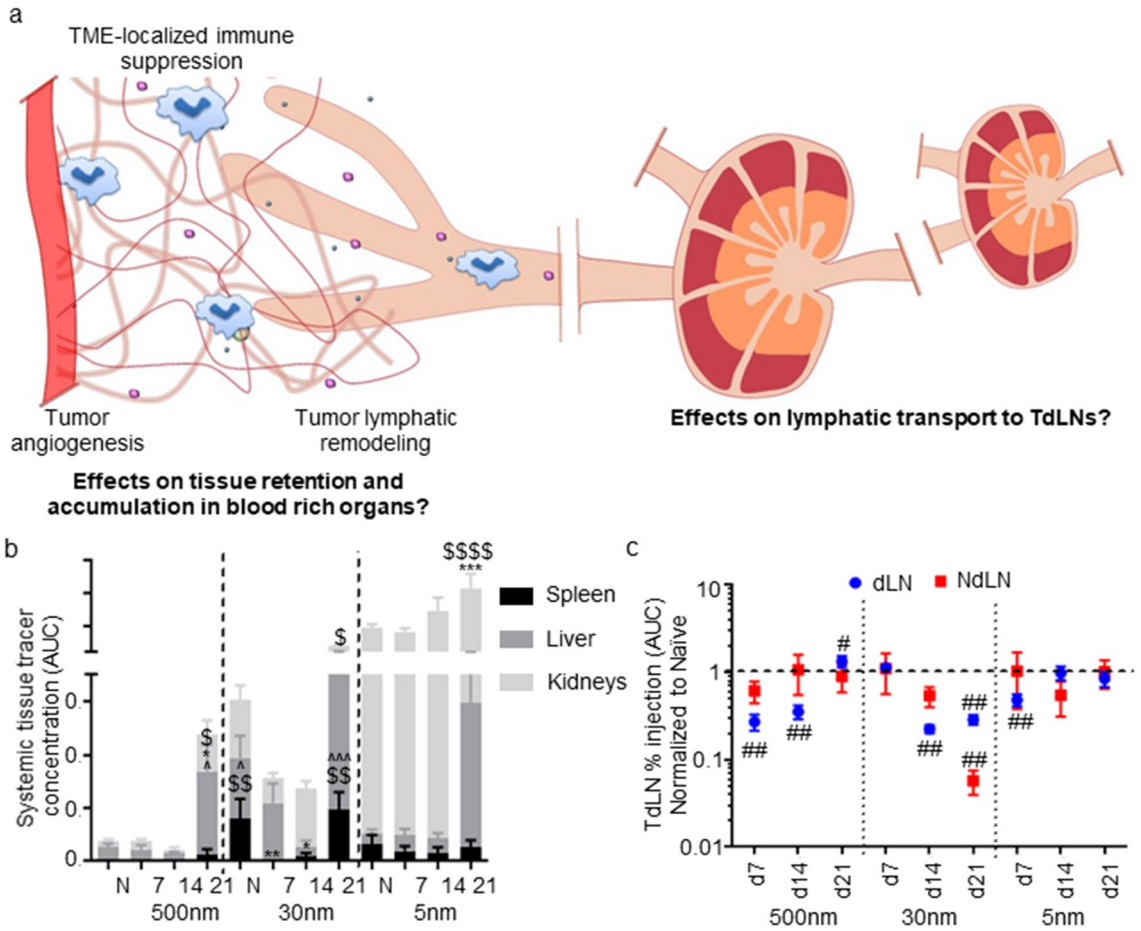

Fig. 4 Molecular dissemination from breast tumors is altered by E0771 disease and progression. **a** Vascular and lymphatic remodeling of the TME may impact molecular dissemination into systemic tissues versus dLN. **b** Tracer accumulation within systemic tissues (spleen, liver, and kidneys) of naïve (N) and d 7, 14, and 21 tumor-bearing animals over 72 h post-injection as quantified as concentration AUC. **c** Relative change in levels of tracer accumulation within the dLN and NdLN over 72 h post-injection quantified as % injection AUC. *Significance relative to naïve, $ indicates significance relative to d7, and ^significance relative to d14 by two-way ANOVA with Tukey's post hoc test; #significance relative to theoretical value of 1.0 by one-sample *t* test; $n = 5–6$ mice

lymphatic uptake, 30 nm tracers accumulated within LN to the highest extents that peaked at 4 h post-injection (Fig. S5d). 5 nm tracers show a similar pattern of dLN access, but at much lower levels (Fig. S5d), while 500 nm tracers show no detectable accumulation until 72 h after injection (Fig. S5d), in line with the slower process of active, cell-mediated transport [52, 57, 58]. 100-fold higher levels of tracer accumulation within LNs i.l. compared to c.l. to the mammary fatpad site of injection are indicative of this transport being lymphatic-mediated (Fig. S5e). 5 nm tracers, which are blood-permeable, rapidly access systemic tissues, followed by a slight decline, while 30 and 500 nm tracers accumulate gradually throughout time in systemic tissues (Fig. S5f). These transport patterns allow for significant concentration (~ 2 orders of magnitude) of 30 nm tracers in the dLN compared to systemic tissues early on; very low concentration of 5 nm tracer in dLN relative to systemic tissues; and a late peak in 500 nm tracer dLN accumulation at 72 h, a time scale consistent with being mediated by lymphatic trafficking cells (Fig. S5g) [52, 57, 58].

This tracer panel was intratumorally (i.t.) injected into animals bearing d7, 14, or 21 E0771 tumors and levels of fluorescent tracer accumulation within each tissue assessed. Retention of 500 nm tracers at the site of injection was largely unchanged throughout tumor progression compared to the naïve mammary fatpad, but 30 and 5 nm tracers were retained to greater extents in d14 versus d14 and 21 tumors, respectively (Fig. 4a, S6). These changes are indicative of altered vascular functions within these diseased tissue microenvironments and consistent with increased tumor vascular volume (d14 and 21) and VEGF-A levels (d21) at these disease stages (Fig. 2a–e). Indeed, accumulation of i.t. injection 5 nm tracers within kidneys, and 500 nm tracers in the liver was increased in late stage (d21) disease (Fig. 4b) when the most profound levels of measured vascular remodeling within the TME were observed (Fig. 2), suggestive of increased clearance into the tumor vasculature. Likewise, 30 nm tracer access to the spleen decreased in d7 and 14 tumors, but increased in late stage (d21) disease when 5 and 500 nm tracer accumulation in blood-rich tissues was increased (Fig. 4b). This increase coincided with increases in PDL1 expression by $CD45^-$ and $CD45^+$ cells within spleens of d21 E0771 tumor-bearing animals (Fig. 3e). Accumulation by mammary fatpad injected tracer within spleens of tumor-bearing relative to naïve mice did not coordinate with increased splenic MDSC frequencies, however. Changes in expression of PDL1 by splenic cells, but not MDSCs are thus synchronous with altered tumor vascular permeability/function profiles in the E0771 TNBC model.

Tumor lymphatic transport was assessed by measurement of accumulation by tracers injected into the mammary fatpad within LNs. 500 nm tracer injected into the mammary fatpad accumulated within TdLNs at reduced levels as early as d7 post-tumor implantation (Fig. 4c). This is suggestive of vascular and lymphatic remodeling of the mammary fatpad induced by the tumor diminishing cell trafficking from the TME, effects sustained at d14 but reversed by d21 (Fig. 4c). Tumors had no effect on 30 nm tracer accumulation within the primary TdLN at early (d7) disease but was dramatically reduced at later stages (Fig. 4c). Accumulation of 5 nm tracer within TdLN was reduced in d7 animals but overall levels were unchanged relative to the naïve (tumor-free) fatpad at later tested stages (Fig. 4c). In support of these observed changes in tracer accumulation being associated with altered tumor lymphatic transport, levels of tracer accumulation within NdLNs remained unchanged irrespective of the tumor, save for reduced levels of 30 nm tracer measured in NdLNs of d21 animals (Fig. 4c). Thus, lymphatic mediated cell trafficking was initially inhibited by tumor growth, but recovered in late stage disease. Lymphatic drainage on the other hand was sustained early in tumor development but then decreased substantially as disease progressed, diminutions that coincided with increased PDL1 expression by $CD45^-$ cells within LNs (Fig. 3d). Immune suppression within the TdLNs is thus coincident with disease stages when tumor antigen would presumably also be locally less abundant.

Primary and secondary TdLNs are niches enriched in factors derived from the TME that support lymphocyte viability, antigen experience, and proliferation

Antitumor immunity has been observed within lymphoid tissues of TNBC patients [7, 25, 31, 32]. The likelihood of priming and cell expansion occurring locally, irrespective of the locally immune suppressed state, within spleens versus LNs within the tumor lymphatic drainage basin was thus evaluated in the E0771 model using the tracer system in two manners. First, when considering local concentrations of accumulating tracers over 72 h after injection into the naïve mammary fatpad, inguinal dLNs were found to be highly enriched (10-, 20-, and twofold for 500, 30, and 5 nm tracers respectively) as compared to systemic tissues such as the spleen (Fig. S7). Relative levels of dLN enrichment also remained high for early (d7) E0771 tumors for all tracer types, and even in d14 tumors for 30 nm tracer (Fig. S7), despite diminished lymphatic transport and increased systemic access by tracers associated with tumor-induced remodeling of the mammary fatpad injection site (Fig. 4b, c). Extratumoral E0771 tumor antigen is thus highly likely to be enriched within TdLNs compared to systemic tissues including spleens.

Second, disease associated changes in transport to axillary LNs that drain the primary LN (inguinal) draining the mammary fatpad (Fig. S4) [59], referred to as the secondary

dLN, were measured in the context of E0771 TNBC to evaluate their potential to support antigenic priming. Accumulation by tracer injected into the naïve mammary fatpad in the secondary dLN followed the same tracer size- and time-dependent trends as the primary dLN, but at a lower magnitude (Fig. S4, S8). 500 nm tracer did not accumulate at measurable levels until 72 h post-injection, consistent with migration being cell-mediated [52, 57, 58]; 30 nm tracer accumulated relatively rapidly; and 5 nm tracer also accumulated rapidly but at a low concentration (Fig. S8). In a tumor context, levels of mammary fatpad injected 30 nm tracer access that is sustained for primary TdLNs were instead enhanced for secondary TdLNs in early stage disease (d7) (Fig. 5a–c, S8). At later stages (d14 and 21) when tracer access to primary TdLNs is substantially reduced, accumulation within secondary TdLNs also diminished, but only to levels similar to that for LNs draining the naïve mammary fatpad (Fig. 5a, b). 500 and 5 nm tracer access to both TdLNs remained low and relatively unchanged (Fig. 5a–c). Thus, lymphatic transport to secondary TdLNs is increased or remains relatively unchanged during disease progression. This is suggestive of the entire lymphatic drainage basin and both (primary and secondary) TdLNs being bathed in tumor-derived material, including tumor antigen. The high level of relative enrichment in factors derived from the TME within primary TdLNs compared to systemic tissues is also seen in secondary TdLNs, save in late stage (d21) disease (Fig. S7).

The relative propensity for various lymphoid tissues to support extratumoral priming by $CD8^+$ T cells against tumor antigen was next assessed by evaluation of responses by CFSE-labeled OT-I $CD8^+$ cells adoptively transferred 2 d prior into E0771-OVA tumor-bearing animals within primary and secondary TdLNs, NdLNs, and spleens. In early d7 E0771 tumors, proliferation was robust in both primary and secondary TdLNs (Fig. 6a, b.i), with a ~ 4 order of magnitude increase in cell density as compared to the TME [peak generation cell count of 200 (Fig. 1) versus 10,000 per 10^6 total live cells]. Proliferation also appeared somewhat more advanced compared to within the TME, with peak generation cell counts being roughly equivalent between G3 and 4 within the primary and secondary TdLNs (Fig. 6b.i) compared to G3 within the TME (Fig. 1e.i). In contrast, proliferation of tumor antigen-specific $CD8^+$ T cells in animals bearing d21 tumors was severely limited by comparison, more closely mirroring cell responses seen within the TME (Fig. 6a, b.ii). Nonetheless, expansion in lymphoid tissues resulted in a higher number of proliferating cells compared to the tumor (Fig. 6c). This led to substantial numbers of tumor-specific T cells in both primary and secondary TdLNs (Fig. 6c). These lymphoid tissue-resident tumor

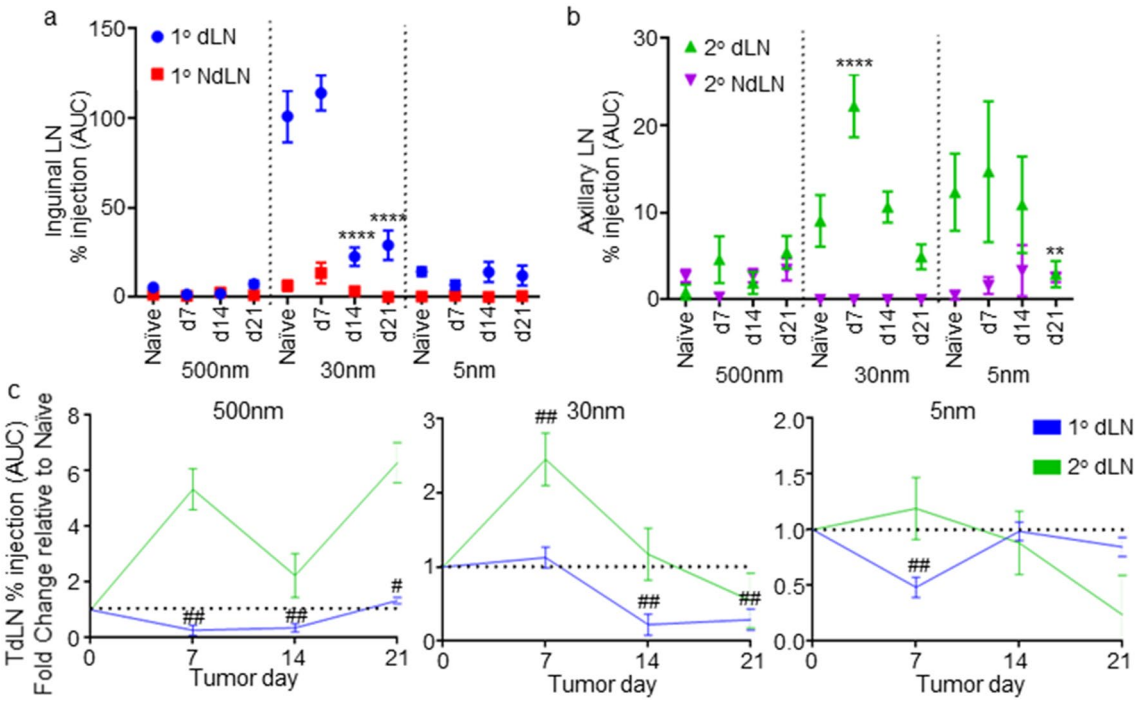

Fig. 5 E0771 disease progression effects on accumulation of intra-fatpad injected tracers within inguinal and axillary LNs. Levels of tracer accumulation within the inguinal (1°) (**a**) and axillary (2°) (**b**) draining and NdLNs over 72 h post-injection during tumor development quantified as % injection AUC. **(c)** Fold change in tracer accumulation within TdLNs over 72 h post-injection in the mammary fatpad (% injection AUC) relative to naïve animals. *Significance relative to naïve by two-way ANOVA with Tukey comparison; #significance relative to theoretical value of 1.0 using one-sample *t* test; $n = 5$–6 mice

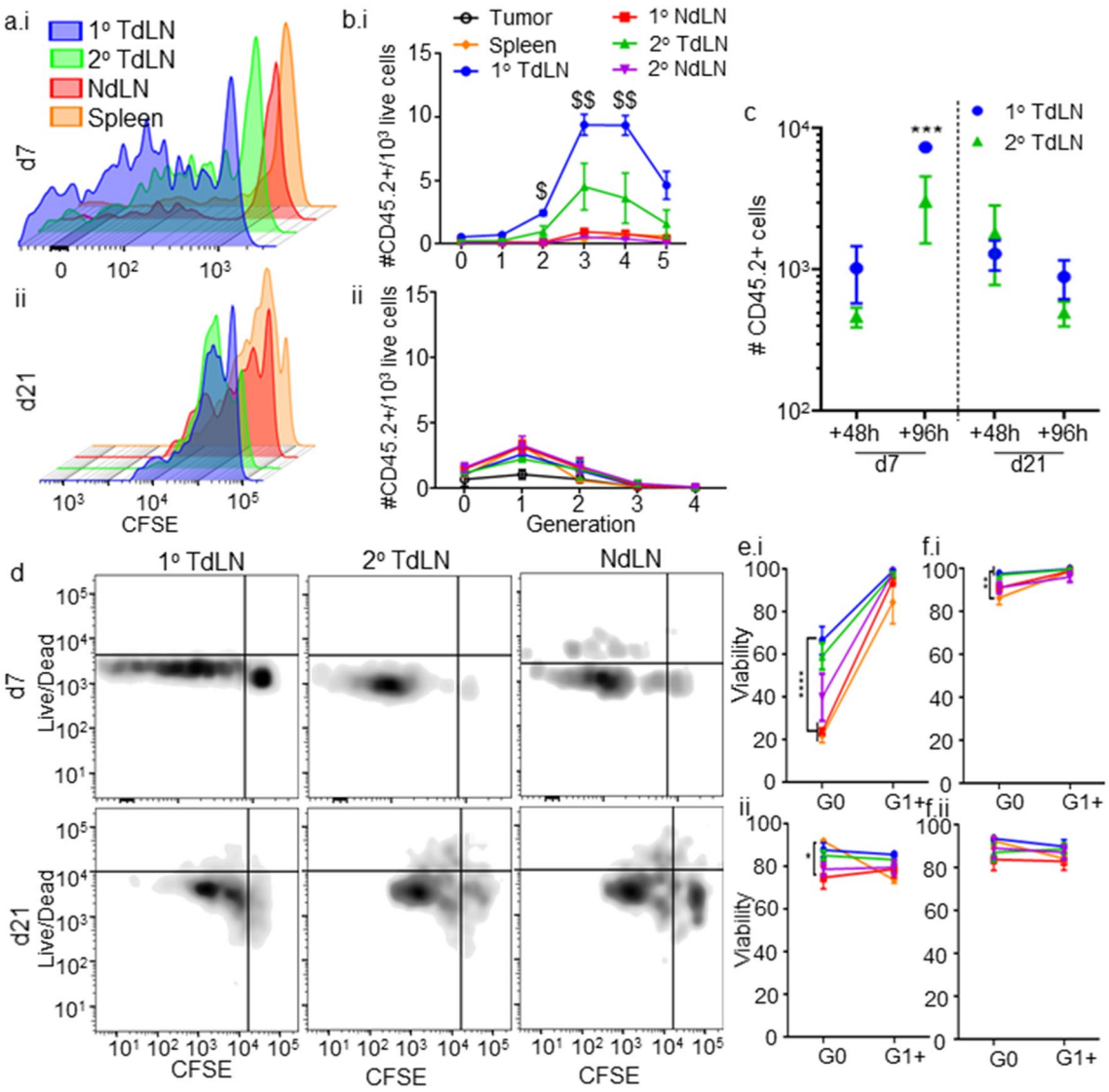

Fig. 6 Tumor antigen-specific T cell priming occurs in E0771 TdLNs. Representative CFSE dilution plots (**a**) and relative density of each proliferative generation per 10^3 cells (**b**) of OT-I CD8 + CD45.2 + donor T cells 48 h post-adoptive transfer into d 7 (i) and 21 (ii) E0771-OVA tumor-bearing CD45.1 animals within lymphoid tissues and TME. Total number (**c**), representative live/dead and CFSE staining flow cytometry plots (**d**), and viability (**e**–**f**) of tumor antigen-specific (OT-I) CD8+CD45.2+ T cells 48 (**c**–**e**) or 96 h (**f**) post-adoptive transfer in 1° (inguinal) and 2° (axial) dLNs (**c**–**f**), NdLNs (**d**–**f**), spleens (**e**–**f**), or TME (**e**–**f**) of d7 or 21 E0771-OVA tumor bearing animals. *Significance by two-way ANOVA with Tukey comparison; $^{\$}$significance against all other groups (including tumor) by RM ANOVA; $n = 5$–6 mice

antigen-specific $CD8^+$ T cells were also largely (> 80%) viable (Fig. 6d, e), with the exception of unproliferated cells 48 h post-transfer into d7 tumor-bearing animals (Fig. 6d, e), in sharp contrast to the low viability of these cells within the TME (Fig. 1d, f). Notably, proliferated and unproliferated donor cells exhibited the highest viability in both primary and secondary TdLNs regardless of tumor stage (Fig. 6d, e). Lymphoid tissues highly enriched in factors derived from the TME thus support both proliferation and viability among tumor-specific T cells, effects diminished in later-stage disease when these environments exhibit immune suppression.

Phenotypes of TME- and lymphoid tissue-resident endogenous cells were also assessed in E0771 tumor-bearing animals. Similar to results in the adoptive transfer model, viable tumor-specific $CD8^+$ T cells within both tumors and primary TdLNs draining early-stage tumors showed high extents of activation ($CD44^+$) and antigen experience ($PD1^+$) (Fig. 7a, b), while cells in the spleen of these animals were primarily naïve ($CD44^-$) (Fig. 7a, b). Within secondary TdLN, roughly 50% of cells were both naïve and antigen-experienced (Fig. 7a, b). As a whole, this indicates that the tumor along with primary

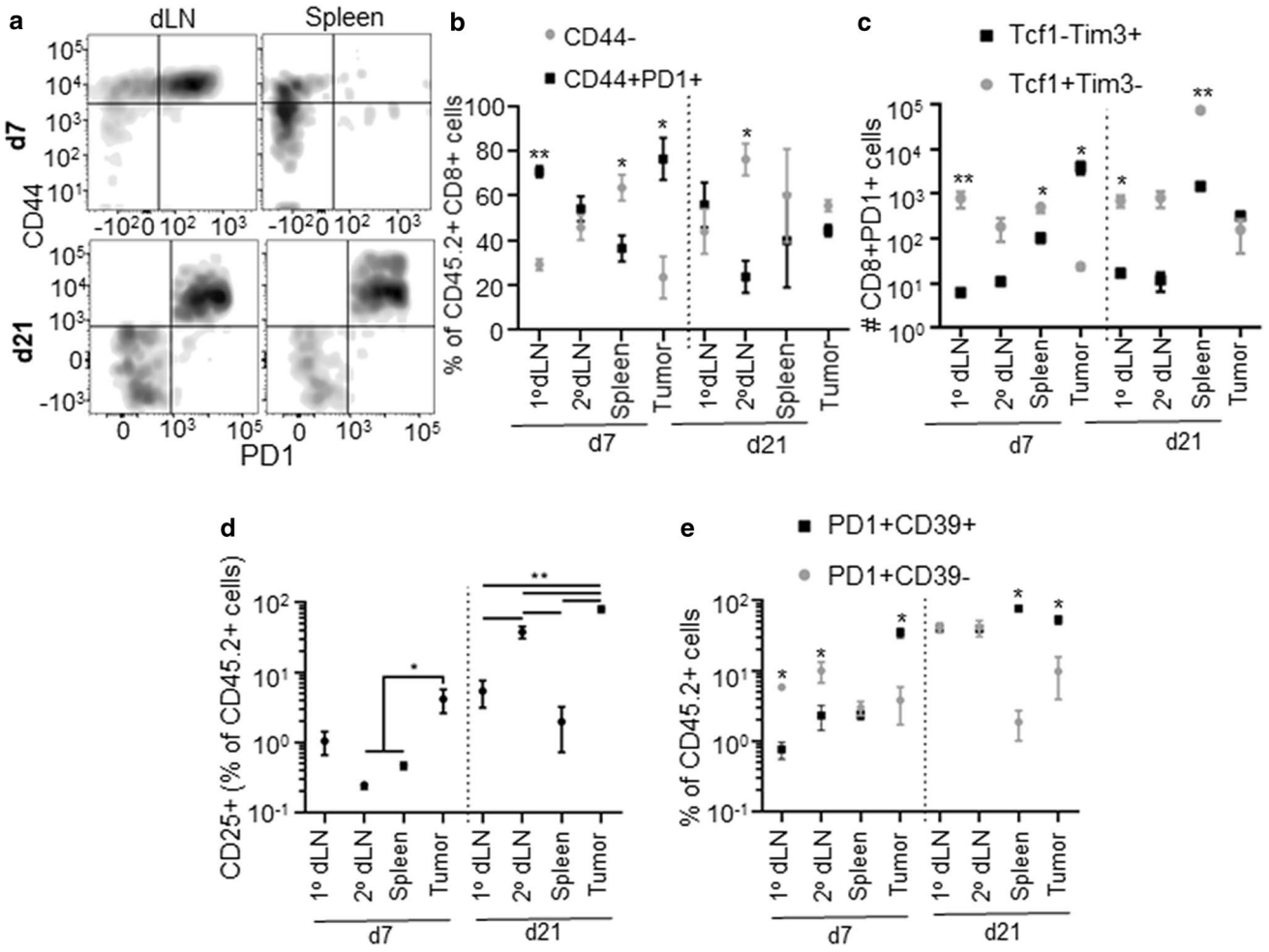

Fig. 7 Quality of endogenous CD8+ T cells within lymphoid tissues and TME changes during E0771 disease progression. Representative CD44 and PD1 staining flow cytometry staining (**a**), fraction of CD44- versus CD44+PD1+ of total CD8+ T cells (**b**), number of Tcf1−Tim3+ or Tcf1+Tim3− PD1+CD8+ T cells (**c**), fraction of CD44+CD25+ cells of CD45.2+ cells (**d**), and fraction of PD1+CD39− versus PD1+CD39+ of CD45.2+CD44+ cells (**e**) in lymphoid tissues (**a**–**e**) or TME (**b**–**e**) of d7 or 21 E0771 tumor bearing animals. *Significance by Mann–Whitney test; $n = 5$–6 mice

and secondary TdLNs demonstrate higher levels of antigen experience in early stage E0771 tumors, while cells in the spleen remain in a more naïve state. In late-stage tumor-bearing animals, on the other hand, $CD8^+$ T cells were more evenly distributed between naïve and antigen-experienced in the primary TdLN and spleen, changes that are coincident with decreased lymphatic drainage and increased levels of splenic accumulation, respectively (Fig. 7a, b). Among $PD1^+$ cells, most tumor-specific cells within lymphoid tissues were in the stem-like ($Tcf1^+Tim3^-$) state [60, 61] in both early and late stage disease (Fig. 7c). However, a majority were $Tim3^+Tcf1^-$, characteristic of an effector/exhausted state [60, 61] in the TME (Fig. 7c). We next analyzed expression of CD25, a marker for activation, and found that $CD44^+$ cells were most activated in the tumor 96 h after transfer on both day 7 and day 21 (Fig. 7d). However, on day 7, cells in the primary TdLN showed slight expansion in activation relative to the secondary TdLN and spleen, and at day 21, cells in the secondary TdLN show high levels of activation. Thus, not only are these cells expanding and experiencing antigen, but they are becoming activated. As exhausted cells can also express activation markers, we next compared CD39 levels, a marker for exhaustion [62]. This revealed that in early stage (day 7) primary and secondary TdLNs, cells were not exhausted (CD39 +), but primarily PD1+CD39−, while cells within the tumor were mostly exhausted (CD39+PD1+) (Fig. 7e). In day 21 tumor-bearing animals, TdLNs harbored a more even split between exhausted and Ag-experienced cells; however, both the spleen contained primarily exhausted cells (Fig. 7e). Thus, cells within the TdLNs are activated and likely to be functional, with the primary and secondary TdLN showing the highest activation at day 7 and 21, respectively, while cells

in the tumor are exhausted. TdLNs thus maintain a population of antigen-experienced CD8$^+$ T cells which have the potential to be invigorated by ICB.

Both primary and secondary TdLNs are therapeutic targets for ICB immunotherapy

The sustained antigen access, increased T cell priming, and delayed onset of immunosuppression in the diseased mammary fatpad dLNs is suggestive of their potential as therapeutic targets in the context of ICB. To test this hypothesis, responses to a single d11 administration of aPD1 ICB directed to the primary (via flank injection) or secondary TdLN (via forelimb injection) compared to systemic administration (i.v. via the jugular vein) were assessed, with isotype mAb control injected in the flank as control (Fig. 8a, b). Previous reports demonstrate that accumulation in LNs draining E0771 tumors is maintained at similar levels in the TdLNs to those shown here in the naïve dLN [63]. Responses to directed delivery revealed by monitoring tumor growth revealed that targeting ICB to either TdLN resulted in transient tumor shrinkage, in contrast to systemic ICB (Fig. 8c). At 5 days after treatment, LN-directed treatment increased the number of granzyme B (GzmB)- expressing effector CD8$^+$ T cells within the TME (Fig. 8d), along with the frequency of actively proliferating (Ki67$^+$) cells (Fig. 8e), compared to treatment with either aPD1 i.p. or isotype i.d. as control. Interestingly, neither the number of GzmB-expressing or frequency of Ki67-expressing CD8$^+$ T cells was unchanged within the primary or secondary

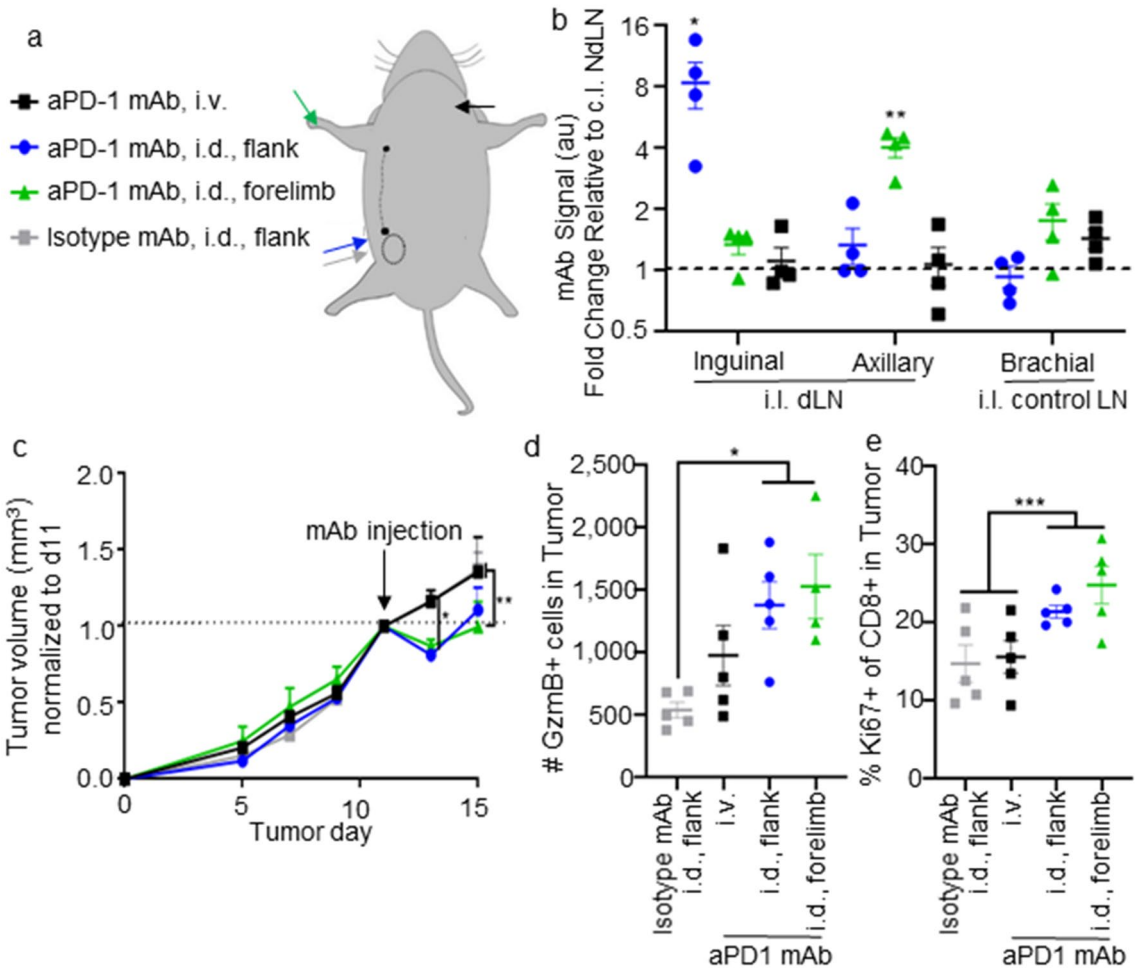

Fig. 8 Locoregional administration of mAb directed to either 1o or 2o TdLN improves therapeutic and immunomodulatory effects of aPD1 ICB. **a** Schematic depicting routes of i.d. injection targeting 1o (blue, gray) or 2o (green) dLNs versus or systemic administration (i.v., black). **b** Fluorescently labelled mAb signal in inguinal, axial, or brachial (as control) LNs 24 h after i.d. injection in the flank (targeting 1o TdLN), i.d. in the forelimb (targeting 2o), or i.v. in the jugular vein relative to LNs contralateral to the tumor (NdLN). **c** Relative tumor size in response to treatment with 100 ug aPD1 mAb on d11. **d–e** Number of granzyme B (GzmB)- (**d**) and Ki67- (**e**) expressing CD8+ T cells in the TME in animals d15 after tumor implantation. * indicates significance by two-way (**a**) or one-way (**b–c**) ANOVA with Tukey comparison; n=5-6 animals.

TdLNs or NdLNs based on the route of administration (Fig. S9). This implies that T cells primed within the dLN after enhanced delivery of aPD1 mAb induces LN-resident T cells to recirculate and reach the TME as functional and proliferating T cells, an interpretation that needs to be confirmed. Thus, by directing ICB mAb to TdLNs, sites of retained antigen access (Fig. 5), sustained proliferation (Fig. 6), and antigen experience (Fig. 5) that results in the generation of a reservoir of tumor-specific stem-like $CD8^+$ T cells (Fig. 7), the response to immunotherapy is enhanced, with resulting functional improvements in T cell phenotype within the tumor itself.

Discussion

TNBC is a deadly disease impacting millions each year, with very few effective therapeutic treatments [1–3]. Immunotherapies have shown clinical benefit in treating many solid tumor malignancies, but the only currently approved ICB therapy for TNBC results in responses in just ~ 16% of patients [6]. A critical hurdle to advancing immunotherapy as an effective approach to combat TNBC is addressing the multiple pathways of immune suppression that result in immunotherapeutic resistance. In particular, there is a growing consensus that T cells require survival niches in order to effectively respond to immunotherapy and result in antitumor effects [64–66]. As such, overcoming immune exclusion and suppression within the TME is a critical hurdle to improving immunotherapeutic efficacy.

Antitumor T cell responses were assessed during tumor progression in the syngeneic E0771 murine model of TNBC and revealed the importance of non-tumor tissues in the development of these responses. As others have shown in additional preclinical tumor models [67] that TME-localized $CD8^+$ T cells exhibit poor viability. Those $CD8^+$ T cells within the TME that are viable also exhibit limited proliferation and an exhausted phenotype. Thus, $CD8^+$ T cells within the TME have a severely diminished likelihood of resulting in robust antitumor effects. In distinct contrast, $CD8^+$ T cell survival was high in LNs draining the TME but not in other LNs or spleens. TdLNs also contained high concentrations of antigen experienced $CD8^+$ T cells, an unsurprising observation given these tissues being highly enriched with factors, such as tumor antigen, derived from the TME by virtue of tumor lymphatic transport. Notably, a high fraction of these cells exhibit a stem-like phenotype, implicating their potential to proliferate and respond to ICB [60, 61]. Indeed, delivery of aPD1 mAb to TdLN using locoregional mAb administration resulted in improved therapeutic effects as compared to conventional systemic (i.p.) therapy that were associated with increased tumor infiltration of degranulated effector ($GzmB^+$) and proliferating ($Ki67^+$) $CD8^+$ T cells. Although the proliferation of TdLN-resident $CD8^+$ T cells decreased with tumor progression, viability and the stem-like phenotype are maintained in late stage disease. These results support the potential for TdLNs as drug targets to improve ICB response rates and efficacy in TNBC, a hypothesis supported by the improved therapeutic effects of TdLN-directed aPD1 in this model.

Tumor development and progression in the syngeneic E0771 murine model of TNBC was shown to result in immune suppression localized to the TME that extended to lymphoid tissues in a manner that was disease stage dependent. Specifically, increased PDL1 expression within spleens and LNs coincided with altered functions of the tumor vasculature that regulate clearance from the mammary fatpad microenvironment, as determined by increased accumulation of i.t. injected tracers in these tissues. Proliferation of tumor antigen-specific $CD8^+$ lymphocytes within both spleens and LNs was also diminished at these disease stages. Remodeling of the tumor vasculature is thus associated with altered immune microenvironments within lymphoid tissues with regulatory functions relevant to antitumor immunity. Unsurprisingly, results also support the concept that these vascular barriers as modulating antigen access within lymphoid tissues. At earlier disease stages when tracer accumulation within systemic tissues and PDL1 expression by cells within spleens was decreased or relatively unchanged, $CD8^+$ T cell priming was modest to low. However, at later stages when the tumor vasculature had most substantially expanded, levels of vascular permeability-enhancing [41–44] VEGF-A were the highest, and i.t. administered tracers accumulated within systemic tissues to the greatest measured extents, antigen experience and proliferation by splenic $CD8^+$ T cells was increased. And though levels of VEGF-C were unchanged during tumor growth, lymphatic drainage was diminished when VEGF-A in the TME was most increased, namely in d14 and 21 E0771 tumors, an observation consistent with the vasculature's role in regulating interstitial pressures and thus the driving force for lymphatic uptake and function [68–70]. Priming of tumor-reactive $CD8^+$ T cells within TdLNs was also sustained in early (d7) but not late (d21) stage when cell mediated or lymphatic drainage transport functions, respectively, were diminished in the tumor. Whether the low extent of $CD8^+$ T cell priming at d21 results from these decreased levels of TdLN accumulation by lymph-accessing species in the TME or coincident local immune suppression, however, remains unresolved. Given the association of $CD8^+$ T cell immunity with TNBC patient survival [29–31], these results are in line with other reports implicating neoangiogenesis as impairing both survival and responses to therapy in breast cancer [46, 47, 71]. How tumor vascular remodeling might be therapeutically mitigated to improve the effects of immunotherapy in TNBC, however, has yet to be systemically explored.

Lymphatic tissues form networks through which antigen can be disseminated, resulting in access by multiple LNs in a network to tumor antigen in order to elicit lymphocyte priming against tumor antigen. This is particularly important in breast cancer, in which the sentinel LN (primary TdLN) is often resected, but secondary TdLNs are left intact given the waning of complete LN dissection [72–74]. In the context of ICB, delivery of aPD1 mAb to either primary or secondary TdLN resulted in improved therapeutic effects compared to conventional systemic therapy. This suggests that locoregional therapy that results in delivery of ICB mAb to LNs draining the TME (either sentinel or secondary TdLNs) is an approach potentially relevant to both neoadjuvant and adjuvant therapy application of ICB when sentinel LN biopsy has been performed.

In conclusion, the potential for lymphoid tissues to mediate extratumoral priming of $CD8^+$ T cell immunity seen in human TNBC patients was evaluated in the syngeneic E0771 mammary carcinoma mouse model. Results in this model demonstrate TdLNs to be lymphoid tissue niches that support the survival and antigenic priming of $CD8^+$ T lymphocytes against lymph-draining antigen. LNs within the tumor lymphatic drainage basin therefore represent a unique, potential tumor immunity reservoir in TNBC for which strategies may be developed to improve the effects of ICB immunotherapy.

Acknowledgements We thank Paul Archer for technical assistance.

Author contributions MJO and SNT designed all experiments and wrote manuscript. MJO carried out all experiments and analyzed all data. MPM assisted in carrying out therapeutic experiments. All authors reviewed and approved the manuscript for submission.

Funding This work was supported by a Komen Foundation Career Catalyst Grant CCR15330478, US National Institutes of Health Grants R01CA207619 (SNT), U01CA214354 (SNT), T32GM008433 (MJO), S10OD016264, and Georgia CORE/It's the Journey. MPM was a National Science Foundation Graduate Research Fellow.

Code availability Not applicable.

Compliance with Ethical Standards

Conflict of interest Not applicable.

Ethics approval All animal work was approved by the Georgia Institute of Technology Institutional Animal Care and Use Committee.

Consent to participate Not applicable.

Consent for publication All authors have reviewed the manuscript and consent to publication.

Availability of data and material Data and materials described here will be made available upon request.

References

1. Siegel RL, Miller KD, Jemal A (2019) Cancer statistics, 2019. CA Cancer J Clin 69:7–34. https://doi.org/10.3322/caac.21551
2. Ferlay J, Soerjomataram I, Dikshit R et al (2015) Cancer incidence and mortality worldwide: sources, methods and major patterns in GLOBOCAN 2012. Int J Cancer 136:E359–E386. https://doi.org/10.1002/ijc.29210
3. Foulkes WD, Smith IE, Reis-Filho JS (2010) Triple-negative breast cancer. N Engl J Med 363:1938–1948
4. Seidel JA, Otsuka A, Kabashima K (2018) Anti-PD-1 and anti-CTLA-4 therapies in cancer: mechanisms of action, efficacy, and limitations. Front Oncol 8:86. https://doi.org/10.3389/fonc.2018.00086
5. Brahmer JR, Tykodi SS, Chow LQM et al (2012) Safety and activity of anti-PD-L1 antibody in patients with advanced cancer. N Engl J Med 366:2455–2465. https://doi.org/10.1056/NEJMoa1200694
6. Schmid P, Adams S, Rugo HS et al (2018) Atezolizumab and nab-paclitaxel in advanced triple-negative breast cancer. N Engl J Med 379:2108–2121. https://doi.org/10.1056/NEJMoa1809615
7. Wang T, Wang C, Wu J et al (2017) The different T-cell receptor repertoires in breast cancer tumors, draining lymph nodes, and adjacent tissues. Cancer Immunol Res 5:148–157. https://doi.org/10.1158/2326-6066.CIR-16-0107
8. Crosby EJ, Wei J, Yang XY et al (2017) Complimentary mechanisms of dual checkpoint blockade expand unique T-cell repertoires and activate adaptive anti-tumor immunity in triple-negative breast tumors. Oncoimmunology 7:e1421891. https://doi.org/10.1080/2162402x.2017.1421891
9. Shiota T, Miyasato Y, Ohnishi K et al (2016) The clinical significance of CD169-positive lymph node macrophage in patients with breast cancer. PLoS ONE 11:1–13. https://doi.org/10.1371/journal.pone.0166680
10. O'Melia MJ, Lund AW, Thomas SN (2019) The biophysics of lymphatic transport: engineering tools and immunological consequences. Science 22:28–43. https://doi.org/10.1016/j.isci.2019.11.005
11. Murphy K, Weaver C (2017) Janeway's Immunobiology, 9th edn. Taylor & Francis, New York
12. Wiig H, Swartz MA (2012) Interstitial fluid and lymph formation and transport: physiological regulation and roles in inflammation and cancer. Physiol Rev 92:1005–1060. https://doi.org/10.1152/physrev.00037.2011
13. Huxley VH, Scallan J (2011) Lymphatic fluid: exchange mechanisms and regulation. J Physiol 589:2935–2943. https://doi.org/10.1113/jphysiol.2011.208298
14. Zawieja DC (2009) Contractile physiology of lymphatics. Lymphat Res Biol 7:87–96. https://doi.org/10.1089/lrb.2009.0007
15. Reddy ST, Van Der Vlies AJ, Simeoni E et al (2007) Exploiting lymphatic transport and complement activation in nanoparticle vaccines. Nat Biotechnol 25:1159–1164. https://doi.org/10.1038/nbt1332
16. Rohner NA, Thomas SN (2016) Melanoma growth effects on molecular clearance from tumors and biodistribution into systemic tissues versus draining lymph nodes. J Control Release 223:99–108. https://doi.org/10.1016/j.jconrel.2015.12.027
17. Rohner NA, Thomas SN (2017) Flexible macromolecule versus rigid particle retention in the injected skin and accumulation in draining lymph nodes are differentially influenced by hydrodynamic size. ACS Biomater Sci Eng 3:153–159. https://doi.org/10.1021/acsbiomaterials.6b00438
18. Allan RS, Waithman J, Bedoui S et al (2006) Migratory dendritic cells transfer antigen to a lymph node-resident dendritic

cell population for efficient CTL priming. Immunity 25:153–162. https://doi.org/10.1016/j.immuni.2006.04.017
19. Thomas SN, Rutkowski JM, Pasquier M et al (2012) Impaired humoral immunity and tolerance in K14-VEGFR-3-Ig mice that lack dermal lymphatic drainage. J Immunol 189:2181–2190. https://doi.org/10.4049/jimmunol.1103545
20. Loo CP, Nelson NA, Lane RS et al (2017) Lymphatic vessels balance viral dissemination and immune activation following cutaneous viral infection. Cell Rep 20:3176–3187. https://doi.org/10.1016/j.celrep.2017.09.006
21. Platt AM, Kutkowski JM, Martel C et al (2013) Normal dendritic cell mobilization to lymph nodes under conditions of severe lymphatic hypoplasia. J Immunol 190:4608–4620. https://doi.org/10.4049/jimmunol.1202600.Normal
22. Nakamura R, Sakakibara M, Nagashima T et al (2009) Accumulation of regulatory T cells in sentinel lymph nodes is a prognostic predictor in patients with node-negative breast cancer. Eur J Cancer 45:2123–2131. https://doi.org/10.1016/j.ejca.2009.03.024
23. Liyanage UK, Moore TT, Joo H-G et al (2002) Prevalence of regulatory T cells is increased in peripheral blood and tumor microenvironment of patients with pancreas or breast adenocarcinoma. J Immunol 169:2756–2761. https://doi.org/10.4049/jimmunol.169.5.2756
24. Danilin S, Merkel AR, Johnson JR et al (2012) Myeloid-derived suppressor cells expand during breast cancer progression and promote tumor-induced bone destruction. Oncoimmunology 1:1484–1494
25. van Pul KM, Vuylsteke RJCLM, van de Ven R et al (2020) Selectively hampered activation of lymph node-resident dendritic cells precedes profound T cell suppression and metastatic spread in the breast cancer sentinel lymph node. J Immunother Cancer 7:133. https://doi.org/10.1186/s40425-019-0605-1
26. Foulds GA, Vadakekolathu J, Abdel-Fatah TMA et al (2018) Immune-phenotyping and transcriptomic profiling of peripheral blood mononuclear cells from patients with breast cancer: identification of a 3 gene signature which predicts relapse of triple negative breast cancer. Front Immunol 9:2028. https://doi.org/10.3389/fimmu.2018.02028
27. Satthaporn S, Robins A, Vassanasiri W et al (2004) Dendritic cells are dysfunctional in patients with operable breast cancer. Cancer Immunol Immunother 53:510–518. https://doi.org/10.1007/s00262-003-0485-5
28. Gil Del Alcazar CR, Huh SJ, Ekram MB et al (2017) Immune escape in breast cancer during in situ to invasive carcinoma transition. Cancer Discov 7:1098–1115. https://doi.org/10.1158/2159-8290.CD-17-0222
29. Mahmoud SMA, Paish EC, Powe DG et al (2011) Tumor-infiltrating CD8+ lymphocytes predict clinical outcome in breast cancer. J Clin Oncol 29:1949–1955. https://doi.org/10.1200/JCO.2010.30.5037
30. Savas P, Virassamy B, Ye C et al (2018) Single-cell profiling of breast cancer T cells reveals a tissue-resident memory subset associated with improved prognosis. Nat Med 24:986–993. https://doi.org/10.1038/s41591-018-0078-7
31. Guo L, Cao C, Goswami S et al (2020) Tumoral PD-1hiCD8+ T cells are partially exhausted and predict favorable outcome in triple-negative breast cancer. Clin Sci 134:711–726. https://doi.org/10.1042/CS20191261
32. Chang AY, Bhattacharya N, Mu J et al (2013) Spatial organization of dendritic cells within tumor draining lymph nodes impacts clinical outcome in breast cancer patients. J Transl Med 11:1–12
33. Duvall CL, Taylor WR, Weiss D, Guldberg RE (2004) Quantitative microcomputed tomography analysis of collateral vessel development after ischemic injury. Am J Physiol Hear Circ Physiol 287:H302–H310. https://doi.org/10.1152/ajpheart.00928.2003
34. Li X, Li M, Lian Z et al (2016) Prognostic role of programmed death ligand-1 expression in breast cancer: a systematic review and meta-analysis. Target Oncol 11:753–761. https://doi.org/10.1007/s11523-016-0451-8
35. Kim IS, Gao Y, Welte T et al (2019) Immuno-subtyping of breast cancer reveals distinct myeloid cell profiles and immunotherapy resistance mechanisms. Nat Cell Biol 21:1113–1126. https://doi.org/10.1038/s41556-019-0373-7
36. Green DR, Droin N, Pinkoski M (2003) Activation-induced cell death in T cells. Immunol Rev 193:70–81. https://doi.org/10.1034/j.1600-065X.2003.00051.x
37. Kabelitz D, Pohl T, Pechhold K (1993) Activation-induced cell death (apoptosis) of mature peripheral T lymphocytes. Trends Immunol 14:338–339
38. Ucker DS, Hebshi LD, Blomquist JE, Torbett BE (1994) Physiological T-cell death: susceptibility is modulated by activation, aging, and transformation, but the mechanism is constant. Immunol Rev 142:273–299. https://doi.org/10.1111/j.1600-065X.1994.tb00893.x
39. Hanahan D, Weinberg RA (2000) The Hallmarks of Cancer. Cell 100:57–70. https://doi.org/10.1007/s00262-010-0968-0
40. Hanahan D, Weinberg RA (2011) Hallmarks of cancer: the next generation. Cell 144:646–674. https://doi.org/10.1016/j.cell.2011.02.013
41. Shibuya M (2011) Vascular endothelial growth factor (VEGF) and its receptor (VEGFR) signaling in angiogenesis: a crucial target for anti- and pro-angiogenic therapies. Genes Cancer 2:1097–1105. https://doi.org/10.1177/1947601911423031
42. Carmeliet P (2005) VEGF as a key mediator of angiogenesis in cancer. Oncology 69:4–10. https://doi.org/10.1159/000088478
43. Nagy JA, Dvorak AM, Dvorak HF (2012) Vascular hyperpermeability, angiogenesis, and stroma generation. Cold Spring Harb Perspect Med 2:1–14. https://doi.org/10.1101/cshperspect.a006544
44. Nagy JA, Feng D, Vasile E et al (2006) Permeability properties of tumor surrogate blood vessels induced by VEGF-A. Lab Investig 86:767–780. https://doi.org/10.1038/labinvest.3700436
45. Schneider BP, Gray RJ, Radovich M et al (2013) Prognostic and predictive value of tumor vascular endothelial growth factor gene amplification in metastatic breast cancer treated with paclitaxel with and without bevacizumab; results from ECOG 2100 trial. Clin Cancer Res 19:1281–1289. https://doi.org/10.1158/1078-0432.CCR-12-3029
46. Su J-C, Mar A-C, Wu S-H et al (2016) Disrupting VEGF-A paracrine and autocrine loops by targeting SHP-1 suppresses triple negative breast cancer metastasis. Sci Rep 6:28888. https://doi.org/10.1038/srep28888
47. Bahnassy A, Mohanad M, Ismail MF et al (2015) Molecular biomarkers for prediction of response to treatment and survival in triple negative breast cancer patients from Egypt. Exp Mol Pathol 99:303–311. https://doi.org/10.1016/j.yexmp.2015.07.014
48. Sweat RS, Sloas DC, Murfee WL (2014) VEGF-C induces lymphangiogenesis and angiogenesis in the rat mesentery culture model. Microcirculation 21:532–540. https://doi.org/10.1111/micc.12132
49. Vaahtomeri K, Karaman S, Mäkinen T, Alitalo K (2017) Lymphangiogenesis guidance by paracrine and pericellular factors. Genes Dev 31:1615–1634. https://doi.org/10.1101/gad.303776.117
50. Lund AW, Wagner M, Fankhauser M et al (2016) Lymphatic vessels regulate immune microenvironments in human and murine melanoma. J Clin Investig 126:3389–3402. https://doi.org/10.1172/JCI79434
51. Stacker SA, Williams SP, Karnezis T et al (2014) Lymphangiogenesis and lymphatic vessel remodelling in cancer. Nat Rev Cancer 14:159–172. https://doi.org/10.1038/nrc3677

52. Kitano M, Yamazaki C, Takumi A et al (2016) Imaging of the cross-presenting dendritic cell subsets in the skin-draining lymph node. Proc Natl Acad Sci 113:1044–1049. https://doi.org/10.1073/pnas.1513607113
53. Pucci F, Garris C, Lai CP et al (2016) SCS macrophages suppress melanoma by restricting tumor-derived vesicle-B cell interactions. Science (80-) 352:242–246. https://doi.org/10.1126/science.aaf1328
54. Hood JL, San Roman S, Wickline SA (2011) Exosomes released by melanoma cells prepare sentinel lymph nodes for tumor metastasis. Cancer Res 71:3792–3801. https://doi.org/10.1158/0008-5472.CAN-10-4455
55. Broggi MAS, Maillat L, Clement CC et al (2019) Tumor-associated factors are enriched in lymphatic exudate compared to plasma in metastatic melanoma patients. J Exp Med 216:1091–1107. https://doi.org/10.1084/jem.20181618
56. Spranger S, Spaapen RM, Zha Y et al (2013) Up-regulation of PD-L1, IDO, and tregs in the melanoma tumor microenvironment is driven by CD8+ T Cells. Sci Transl Med. https://doi.org/10.1126/scitranslmed.3006504
57. Platt AM, Randolph GJ (2013) Dendritic cell migration through the lymphatic vasculature to lymph nodes, 1st edn. Elsevier Inc., Amsterdam
58. Schineis P, Runge P, Halin C (2019) Cellular traffic through afferent lymphatic vessels. Vasc Pharmacol 112:31–41. https://doi.org/10.1016/j.vph.2018.08.001
59. Harrell MI, Iritani BM, Ruddell A (2008) Lymph node mapping in the mouse. J Immunol Methods 332:170–174. https://doi.org/10.1016/j.jim.2007.11.012
60. Im SJ, Hashimoto M, Gerner MY et al (2016) Defining CD8+T cells that provide the proliferative burst after PD-1 therapy. Nature 537:417–421. https://doi.org/10.1038/nature19330
61. Miller BC, Sen DR, Al Abosy R et al (2019) Subsets of exhausted CD8+ T cells differentially mediate tumor control and respond to checkpoint blockade. Nat Immunol 20:326–336. https://doi.org/10.1038/s41590-019-0312-6
62. Gupta PK, Godec J, Wolski D et al (2015) CD39 expression identifies terminally exhausted CD8+ T cells. PLoS Pathog 11:1–21. https://doi.org/10.1371/journal.ppat.1005177
63. Francis DM, Manspeaker MP, Schudel A et al (2020) Blockade of immune checkpoints in lymph nodes through locoregional delivery augments cancer immunotherapy. Sci Transl Med 12:eaay3575
64. Jansen CS, Prokhnevska N, Master VA et al (2019) An intratumoral niche maintains and differentiates stem-like CD8 T cells. Nature 576:465–470. https://doi.org/10.1038/s41586-019-1836-5
65. Cabrita R, Lauss M, Sanna A et al (2020) Tertiary lymphoid structures improve immunotherapy and survival in melanoma. Nature 577:561–565. https://doi.org/10.1038/s41586-019-1914-8
66. Petitprez F, de Reyniès A, Keung EZ et al (2020) B cells are associated with survival and immunotherapy response in sarcoma. Nature 577:556–560. https://doi.org/10.1038/s41586-019-1906-8
67. Horton BL, Williams JB, Cabanov A et al (2018) Intratumoral CD8+ T-cell apoptosis is a major component of T-cell dysfunction and impedes antitumor immunity. Cancer Immunol Res 6:14–24. https://doi.org/10.1158/2326-6066.CIR-17-0249
68. Cursiefen C, Chen L, Borges LP et al (2004) VEGF-A stimulates lymphangiogenesis and hemangiogenesis in inflammatory neovascularization via macrophage recruitment. J Clin Investig 113:1040–1050. https://doi.org/10.1172/JCI200420465.1040
69. Hirakawa S, Kodama S, Kunstfeld R et al (2005) VEGF-A induces tumor and sentinel lymph node lymphangiogenesis and promotes lymphatic metastasis. J Exp Med 201:1089–1099. https://doi.org/10.1084/jem.20041896
70. Halin C, Tobler NE, Vigl B et al (2007) VEGF-A produced by chronically inflamed tissue induces lymphangiogenesis in draining lymph nodes. Blood 110:3158–3167. https://doi.org/10.1182/blood-2007-01-066811
71. Rahma OE, Hodi FS (2019) The intersection between tumor angiogenesis and immune suppression. Clin Cancer Res 25:5449–5457. https://doi.org/10.1158/1078-0432.CCR-18-1543
72. Naik AM, Fey J, Gemignani M et al (2004) The risk of axillary relapse after sentinel lymph node biopsy for breast cancer is comparable with that of axillary lymph node dissection. Ann Surg 240:462–471. https://doi.org/10.1097/01.sla.0000137130.23530.19
73. Pesce C, Morrow M (2013) The need for lymph node dissection in nonmetastatic breast cancer. Annu Rev Med 64:119–129. https://doi.org/10.1146/annurev-med-052511-135500
74. Giuliano AE, Hunt KK, Ballman KV et al (2011) Axillary dissection vs no axillary dissection in women with invasive breast cancer and sentinel node metastasis. J Am Med Assoc 305:569–575. https://doi.org/10.1001/jama.2011.90